Biomaterials 226 (2020) 119543

Contents lists available at ScienceDirect

Biomaterials

journal homepage: www.elsevier.com/locate/biomaterials

Non-invasive *in vivo* imaging of caspase-1 activation enables rapid and spatiotemporal detection of acute and chronic inflammatory disorders

Young Ji Ko[a,b,1], Jae-Won Lee[c,d,1], Eun-Jeong Yang[d,e,1], Nayoon Jang[c,d], Jooho Park[b], Yoon Kyung Jeon[f], Je-Wook Yu[g], Nam-Hyuk Cho[c,d,h,*,2], Hye-Sun Kim[d,e,i,**,2], Ick Chan Kwon[a,b,j,***,2]

[a] KU-KIST Graduate School of Converging Science and Technology, Korea University, Seoul, 02841, Republic of Korea
[b] Biomedical Research Institute, Korea Institute of Science and Technology (KIST), Seoul, 02792, Republic of Korea
[c] Department of Microbiology and Immunology, Seoul National University College of Medicine, Seoul, 03080, Republic of Korea
[d] Department of Biomedical Sciences, Seoul National University College of Medicine, Seoul, 03080, Republic of Korea
[e] Department of Pharmacology, Seoul National University, College of Medicine, Seoul, 03080, Republic of Korea
[f] Department of Pathology, Seoul National University College of Medicine, Seoul, 03080, South Korea
[g] Department of Microbiology and Immunology, Yonsei University College of Medicine, Seoul, 03722, South Korea
[h] Institute of Endemic Disease, Seoul National University Medical Research Center and Bundang Hospital, Seoul, 03080, South Korea
[i] Seoul National University College of Medicine, Bundang Hospital, Sungnam, 13620, Republic of Korea
[j] KIST-DFCI On-Site-Lab, Department of Cancer Biology, Dana-Farber Cancer Institute, Harvard Medical School, Boston, MA, 02215, USA

ARTICLE INFO

Keywords:
Inflammasome
Caspase-1
Activatable fluorescence probe
Inflammation
Cancer
Alzheimer's disease

ABSTRACT

Inflammasome plays a critical role in diverse inflammatory disorders, including cancers and Alzheimer's disease. It is induced by various pathogenic insults and activates caspase-1, a hallmark executor of inflammasome. Here, we developed an activatable fluorescence probe for visualization of active caspase-1. This caspase-1 probe is biocompatible, efficiently delivered into cells and tissues, and specifically emits fluorescence upon caspase-1 activation as assessed in *in vitro* and *in vivo* models of inflammatory conditions. We demonstrated efficient *in vivo* imaging of caspase-1 activation in early stages of various inflammatory conditions of mice models, including endotoxin shock, inflammatory bowel disorder, transplanted cancer, and Alzheimer's disease. Notably, the caspase-1 probe enables detection of neuroinflammation *in vivo* two months earlier than cognitive impairments occur in Alzheimer's disease model. We detected significant fluorescence emitted from inflamed sites, as well as their draining lymph nodes, by macroscopic imaging analysis within 30 min after systemic injection of the probe. This novel synthetic probe could be applied for efficient and rapid detection of caspase-1 activity in a spatiotemporal way by non-invasive imaging.

1. Introduction

The inflammasome is a multi-protein intracellular complex that responds to pathogens and sterile stressors via detection of pathogen-associated molecular patterns (PAMPs) and danger-associated molecular patterns (DAMPs) [1–3]. Upon activation, it induces expression of highly pro-inflammatory cytokines, including interleukin-1β (IL-1β) and IL-18, as well the pathway for a proinflammatory form of regulated cell death, pyroptosis. In detail, this molecular machine comprises of a receptor that senses PAMPs and/or DAMPs, an adaptor molecule known as ASC (apoptosis-associated speck-like protein containing a caspase activation and recruitment domain), and a zymogen procaspase-1 [3]. Recognition of exogenous and/or endogenous stimuli generated by physiological and pathogenic stresses nucleates ASC to form discrete foci, or specks, within the activated cell. Caspase-1 is then recruited and undergoes autocatalytic cleavage to produce active caspase-1. The active subunits of caspase-1 can proteolytically process cytokines, IL-1β and IL-18, to be secreted and trigger pyroptosis through cleavage of

* Corresponding author. Department of Microbiology and Immunology, Seoul National University College of Medicine, Seoul 03080, Republic of Korea.
** Corresponding author. Department of Biomedical Sciences, Seoul National University College of Medicine, Seoul, 03080, Republic of Korea.
*** Corresponding author. KU-KIST Graduate School of Converging Science and Technology, Korea University, Seoul, 02841, Republic of Korea.
E-mail addresses: chonh@snu.ac.kr (N.-H. Cho), hyisun@snu.ac.kr (H.-S. Kim), ikwon@kist.re.kr (I. Chan Kwon).
[1] These authors contributed equally.
[2] These authors jointly supervised this work.

https://doi.org/10.1016/j.biomaterials.2019.119543
Received 28 July 2019; Received in revised form 7 October 2019; Accepted 10 October 2019
Available online 11 October 2019

Gasdermin D [4,5]. Even though multiple molecular sensors, including NOD-like receptor (NLR) family members, are involved in initiating the inflammasome activation pathway, activated caspase-1 is a hallmark executor of this pathway [3,6,7]. Recent advances highlight the involvement of this molecular sentinel with fundamental immunological processes and its functional importance in maintaining homeostasis of diverse biological functions [3]. In addition, dysregulation of inflammasome is associated with the initiation and progression of a number of inflammatory syndromes with a high impact on public health, such as metabolic disorders, cancers, neurodegenerative diseases, as well as microbial infections [8–11]. Therefore, development of promising therapeutics that target inflammasome activity in various inflammatory diseases has attracted considerable attention in recent years [8,12–14].

Detection of inflammasome activation *in vitro* and *in vivo* may also provide enormous advantages for mechanistic studies, diagnosis, drug discovery, and therapeutic monitoring in inflammatory disorders, given its wide and significant role in innate immune response, shaping adaptive immunity, and clearance of pathogenic insults [8,12]. However, the absence of *in vivo* monitoring techniques has limited our understanding of the location and timing of inflammasome activity at the tissue or organism level. Only a few recent studies have established an *in vivo* reporter system to visualize inflammasome activation in real-time and have just started to dissect its influence on the immune system [15–17]. For example, a recent study using a live ASC reporter in genetically-modified zebrafish showed that a toxic stimulus triggered ASC speck formation and rapid pyroptosis in keratinocytes *in vivo*, and that macrophages engulfed and digested the speck-containing, pyroptotic debris [17]. This *in vivo* imaging demonstration of ASC speck formation by keratinocytes in response to inflammatory conditions and subsequent pyroptosis, underscores the relevance of inflammasome signaling in epithelia [17]. In addition, another study generated chimeric mice expressing ASC-GFP in hematopoietic stem cells to visualize the spatiotemporal dynamics of inflammasome activation *in vivo* [15]. They found that transient inflammasome activation in subcapsular sinus macrophages in draining lymph node is functionally associated with an influx of inflammatory cells and an increase in the magnitude of T cell response upon local vaccinia virus infection [15]. Nevertheless, all these currently available imaging techniques only target ASC and requires genetic modification of cells or organisms to visualize *in vivo* dynamics of inflammasome activation. Therefore, quantitative analysis of inflammation activation *in vivo* is technically limited and requires microscopic access to the target cells and tissues for visualization of ASC speck formation. Targeting the enzymatic activity of caspase-1 is an alternative since caspase-1 is a hallmark cysteine protease activated by all the inflammasome pathways [4]. However, current methods measuring caspase-1 activity generally require cellular lysis or genetic modification, thereby have limited direct application *in vivo* [15,18].

In this study, we developed a novel fluorescent probe which can emit near infrared (NIR) radiation upon specific cleavage by active caspase-1 and applied it as imaging sensor for inflammasome activation. *In vivo* applicability of the caspase-1 sensor was examined in various acute and chronic inflammatory disorders, including endotoxin stimulation, inflammatory bowel disease (IBD), grafted cancer, and Alzheimer's disease (AD), via non-invasive fluorescence imaging. Our results show that the synthetic fluorescent probe enables quantitative analysis of spatiotemporal dynamics *in vivo* inflammasome activation without invasive treatment. Furthermore, efficient visualization of inflammasome activity enable early detection of inflammatory sites and their draining lymph nodes before manifestation of systemic signs or symptoms in the specific disorders. Therefore, our probe system could provide a novel platform to detect *in vivo* dynamics of active inflammasome for diagnosis, drug discovery, and therapeutic monitoring in various inflammatory conditions.

2. Materials and methods

2.1. Reagents and antibodies

Cy5.5 (Flamma® carboxylic acid, maximum excitation/emission wavelength: 675nm/695 nm), a water-soluble and near infrared (NIR) dye, was purchased from Bioacts (Incheon, Republic of Korea) and activated to *N*-hydroxysuccinamide (NHS) groups using Dipyrrolidino (*N*-succinimidyloxy) carbenium hexafluorophosphate (HSPyU) (St. Louis, MO, USA) to conjugate to the amine group of peptide substrate. Black hole quencher-3 (BHQ®-3, quenching range: 620–730 nm with maximum absorption at 672 nm) coupled with NHS was obtained from Bioresearch Technologies (Petaluma, CA, USA). The caspase-1 substrate peptide (G-W-E-H-D-G-K) protected by tert-Butyloxycarbonyl (Boc), *tert*-Butyl (*t*Bu), and Trityl (Trt) groups in amine or carboxyl group of each amino acid (H_2N-G-W[Boc]-E[*t*Bu]-H[Trt]-D[*t*Bu]-G-K-OH, Supplementary Fig. 1) was purchased from Peptron (Daejeon, Republic of Korea). Caspase-1, caspase-3, caspase-8, and caspase-11 were purchased from Enzo Life Science (Farmingdale, NY, USA). Caspase-1 inhibitor, Ac-YVAD-cmk, was obtained from Invivogen (San Diego, CA, USA). Fetal bovine serum (FBS) and Roswell Park Memorial Institute (RPMI) 1640 medium were purchased from Gibco (Carlsbad, CA, USA). Dulbecco's modified Eagle's medium (DMEM) was purchased from Thermo Scientific (Waltham, MA, USA). Lipopolysaccharides (LPS) and adenosine triphosphate (ATP) were obtained from Sigma-Aldrich (St. Louis, MO, USA). Dextran sodium sulfate (DSS) was purchased from MP Biomedical (Santa Ana, CA, USA). 4′,6-diamidino-2-phenylindole dihydrochloride (DAPI) was purchased from Thermo Scientific.

2.2. Synthesis and characterization of caspase-1 activatable probe

The caspase-1 activatable (Cas-1) probe was synthesized by conjugating Cy5.5 and BHQ-3 to caspase-1 substrate (G-W-E-H-D-G-K) (Supplementary Fig. 1). First, BHQ-3-NHS was attached to an amine group of lysine (K) of caspase-1 peptide substrate. Second, protecting groups were removed with trifluoroacetic acid (TFA)/distilled water (DW)/Anisol (95:2.5:2.5). Third, the Cy5.5-NHS was attached to the *N*-terminal of the caspase-1 substrate peptide. Active caspase-1 recognizes WEHD sequence and cleaves site after aspartate (D) [19]. The synthetic Cas-1 probe was characterized by analytical reverse phase-high performance liquid chromatography on C18 column (RP-HPLC, Agilent Tech, Santa Clara, CA, USA), UV–vis spectrofluorometer (F-7000 Fluorescence Spectrophotometer; Hitach, Tokyo, Japan), and matrix-assisted laser desorption/ionization-time of flight mass spectrometry (MALDI-TOF MS, Microflex LRF20, Bruker Daltonics, Bremen, Germany) (Supplementary Fig. 2). The molecular weight (2.255 kDa) of the synthetic probe was confirmed by mass spectrometry and the purity (> 90%) was analyzed by HPLC (Supplementary Figs. 2a and b). The chemical structure of the Cas-1 probe was confirmed by proton nuclear magnetic resonance spectroscopy (^{1}H NMR, DD2 600 MHz FT NMR, Agilent Technologies, USA) using Cy5.5 (3 mg/ml), BHQ-3 (3 mg/ml), and Cas-1 probe (6 mg/ml) dissolved in DMSO-d_6 (Supplementary Fig. 2c). To confirm the specificity of the Cas-1 probe, it was incubated for 2 h at 37 °C in the presence of 5 unit/ml of caspase-1, caspase-3, caspase-8, caspase-11, or caspase-1 plus caspase-1 inhibitor, Ac-YVAD-cmk (20 μg/ml). Fluorescence intensity was then measured in a caspase activation buffer (50 mM N-2-hydroxyethylpiperazine-*N*′-2-ethanesulfonic acid (HEPES), pH 7.2, 50 mM sodium chloride, 0.1% 3-[(3-Cholamidopropyl) dimethylammonio]-1-propanesulfonate (CHAPS), 10 mM ethylenediaminetetraacetic acid (EDTA), 5% glycerol, and 10 mM dithiothreitol) The Cas-1 probe (2 μg/ml) was also incubated in the activation buffer containing various concentration (0, 2.5, 5, 7.5, 10 unit/ml) of caspase-1 enzyme for 60 min. The excitation wavelength was fixed at 675 nm and emission wavelength measured from 676 nm to 800 nm for detection of fluorescence radiation by a spectrofluorometer. A synthetic Cas-3 probe (Cy5.5-G-D-E-V-

D-G-K-BHQ-3, substrate sequence underlined) was prepared as previously described [20], and used as the control probe.

2.3. Cell culture, cytotoxicity, and hemocompatibility of caspase-1 activatable probe

Human monocyte cell line, THP-1 (Korean Cell Line Bank, Seoul, Republic of Korea) was maintained in RPMI 1640 medium containing 10% (v/v) FBS, 1% (v/v) antibiotics/antimycotics (Welgene Inc, Gyeongsan, Republic of Korea), and 10 mM HEPES at 37 °C. Bone marrow derived macrophages (BMDMs) were harvested from mice hind leg bones. BMDMs were cultured for 7 d with macrophage colony-stimulating factor (M-CSF, Peptron, Daejeon, Republic of Korea) in RPMI 1640 medium containing 10% (v/v) FBS and 1% (v/v) antibiotics/antimycotics. MC38 colon adenocarcinoma [21] cells were cultured in DMEM with 10% FBS and 1% antibiotics/antimycotics. The cytotoxicity of the Cas-1 probe was evaluated by Cell Counting Kit-8 (CCK-8, Sigma-Aldrich). In brief, BMDMs or THP-1 cells (1×10^4 cells/well) were seeded in 96-well microplate. Various concentrations of the Cas-1 probe (5, 10, 25, 50, and 100 μg/ml) were added to the cell culture and incubated for 24 h. The absorbance of CCK-8 solution was observed at 450 nm with a plate reader (Molecular Devices, CA, USA). In order to examine the hemocompatibility of the Cas-1 probe, we performed *in vitro* hemolysis assay and *in vivo* hematological analysis. Hemolytic activity of the synthetic probe was evaluated by assessing mouse red blood cells (RBCs). Briefly, mouse blood was harvested in heparinized tubes and RBCs were collected using Ficoll-paque PLUS density gradient media (GE healthcare, Chicago, IL, USA) according to the manufacturer's instruction. Fresh RBCs in suspension were incubated with the Cas-1 probes at various concentrations (10, 20, 40, and 80 μM which are equivalent to 22.5, 45.0, 90.0, and 180.0 μg/ml, respectively) at room temperature for 1 h and centrifuged to collect the supernatants. RBCs suspended in phosphate-buffered saline (PBS) and DW were used as negative and positive control, respectively. The levels of released hemoglobin in the supernatant solutions were assessed by measuring absorbance at 540 nm using a microplate reader (Tecan, Mannedorf, Switzerland). The hemolytic ratio was calculated as follows: % hemolysis ratio = $O.D._{Test}/O.D._{Positive\ control}$ x 100. The number of RBCs collected by centrifugation was also counted by using hemocytometer (Paul Marienfeld GmbH & Co. KG, Lauda-Königshofen, Germany). Hematological changes were examined in mice injected with the Cas-1 probe. The synthetic probe (100 μg/100 μl of saline) was intravenously injected via tail vein and whole blood was collected at 2 h after probe injection to measure complete blood counts (CBC). Analysis of CBC was performed using ADVIA 2012i Hematology System (Siemens Healthineers, Erlangen, Germany).

2.4. In vitro imaging, flow cytometry, and enzyme-linked immune sorbent assay (ELSIA)

BMDMs or THP-1 cells (2×10^5 cells/dish) were seeded in 35 mm coverslip bottom dishes and cultured for overnight. Then, cells were incubated in RPMI 1640 medium containing the Cas-1 or Cas-3 probe (1.5 μg/ml). After 30 min of incubation, LPS (1.5 μg/ml) was treated for 3 h followed by ATP (5 mM) for 30 min. Cells were then fixed in absolute methanol and incubated with DAPI for nuclear staining for 10 min. Cells were observed under a confocal microscope (Leica, Wetzlar, Germany). For flow cytometric analysis, stimulated cells were fixed with 4% paraformaldehyde and fluorescence intensities were examined on a FACS Fortessa II flow cytometer (BD Biosciences). Data were analyzed using Flowjo software (Tree Star, Ashland, OR, USA). Concentration of IL-1β in cell culture supernatants was also measured by mouse IL-1β ELISA kits, according to manufacturer's instruction (Biolegend, San Diego, CA, USA). The amount of IL-1β, IL-6, and tumor necrosis factor (TNF)-α in mice sera were determined by Bio-Plex ProTM cytokine assay system (Bio-Rad, Hercules, CA, USA).

2.5. Animal experiments

Mice (Orient Bio, Seoul, South Korea) were housed and maintained in the specific pathogen-free facility at Seoul National University (SNU) College of Medicine and Korea Institute of Science and Technology (KIST). Animal experiments were performed after approval by SNU and KIST IACUC (permission ID: SNU-180410-3, SNU-161223-1-2, SNU-180410-3, KIST-2018-096). Caspase-1/11 knockout (KO) mice (B6N.129S2-Casp1tm1Flv/J) were purchased from Jackson Laboratories (Bar Harbor, ME, USA). These mice were bred with homozygous mice and genotyped by polymerase chain reaction (PCR). C57BL/6 mice were utilized for inflammation models and control experiments as indicated. For endotoxin stimulation, mice were injected with LPS (5 μg/mouse) and ATP (5 mg/mouse) in right footpad and observed at the indicated time. Acute colitis was induced through the oral intake of 3% DSS in fresh tap water *ad libitum* for the indicated time. The mice were monitored daily and applied for imaging analysis. For tumor models, athymic nude mice (six to eight week old, Nara biotech, Seoul, Republic Korea) were subcutaneously injected with MC38 cells (5×10^6 cells/mouse) into the flank of mice or intravenously (5×10^5 cells/mouse) via the lateral tail vein. Then, mice were monitored every five days after tumor injection. For AD model, 5x familial AD (5xFAD) mice (B6SJL-Tg [APPSwFlLon, PS1*M146L*L286V] 6799Vas/J, Jackson Laboratories) were maintained by crossing the hemizygous transgenic mice with B6SJL F1 mice (Jackson Laboratories) [22]. Transgenic mice were identified by PCR, and non-transgenic littermates were used as controls. 5xFAD mice express both mutant human APP695, which harbors the Swedish mutation (K670 N, M671L), Florida mutation (I716V), and London mutation (V717I), and human PS1 with two FAD mutations (M146L and L286V). T-maze and Y-maze were performed in the animal behavior laboratory in SNU. T-maze was made of black acrylic plastic (each arm 30 × 15 × 7 cm and 7 × 7 cm center piece). At the start of the trials, mice were placed into the start arm facing away from the goal arms, after 30 min habitation in an animal behavior testing room. Each mouse could freely explore and to choose the left or right goal arm. Goal arms were closed using the center piece after the tail cleared the goal arm. After 30 s, the center piece was removed, and the mouse was moved back into the start arm to choose again between the two open goal arms. Two T-maze test trials were performed each day with at 1 h intervals for 3 consecutive days, and scored as previously described [23]. If the mouse repeatedly chose the same goal arm in the same trial, it scored 0, and if it selected a different goal arm, a score of 1 was given. Y-maze consists of 3 equal arms (40 × 15 × 9 cm) using black acrylic plastic [24]. After 10 min habitation, mice were placed into the center of Y-maze at the start of the trial. Mice could freely explore the three arms for 8 min. All movements were recorded by video camera and alternation ratio, which were used to evaluate number of arm entries in triplicates.

2.6. In vivo and ex vivo imaging

For sepsis model, the Cas-1 probe (100 μg/100 μl of saline/mouse) was intravenously injected via tail vein at the indicated time after LPS and ATP treatment. Live mice or lymph nodes collected from sacrificed animals were imaged by an IVIS-Lumina Series III (Caliper Life Science, Hopkinton, MA, USA) at the indicated time after the probe injection. For DSS-induced colitis model, the Cas-1 probe was intravenously injected at the indicated time after DSS treatment and live mice or collected tissues from sacrificed mice were analyzed by IVIS-Lumina system at the indicated time after Cas-1 probe injection. Mice transplanted with tumor cells were imaged by IVIS-Lumina or eXplore Optix system (Advanced Research Technologies, Montreal, Canada) at 2 and 4 h after Cas-1 probe injection, respectively. In AD model imaging, 5xFAD mice (three to six months old) were analyzed each month. The Cas-1 probe was intravenously injected and *in vivo* images were taken

every 30 min by eXplore Optix system starting at 2 h after probe injection. Animals were also humanely sacrificed and collected brains and lymph nodes were imaged by an IVIS-Lumina system. For non-invasive imaging, animals were shaved before imaging process by IVIS-Lumina system. In case of head imaging in AD model by eXplore Optix system, we partially cut the skin to expose mouse skull. The fluorescence intensity of region of interest (ROI) was calculated using the Living Image software (for IVIS-Lumina, radiation efficiency = [photons/s]/[μW/cm^2]; PerkinElmer, Boston, MA, USA) or Analysis Workstation software program (for eXplore Optix system, radiation efficiency = total photons/unit area; Advanced Research Technologies, Montreal, Canada), as previously described [20,25]. Imaging analysis of all the mice and their tissues to be compared was performed under the same settings and conditions of the imaging systems. To define brain-draining lymph nodes, 1 μl of solution containing Cy5.5 and 10% of Evans blue dye was injected into ventricular zones of animals by stereotaxic surgery. 26-gauge syringes (Hamilton, Nevada, USA) were used to inject into lateral ventricles (coordinate from bregma: AP -0.46 mm, ML ± 1.0 mm, DV – 2.5 mm). In order to examine whether the Cas-1 probe without BHQ-3 could pass through the blood brain barrier (BBB), Cy5.5 dye conjugated with G-W-E-H-D-G-K peptide (80 μg/mouse) was intravenously administered to 3 month- and 6 month-aged 5xFAD mice and fluorescent signals from their brains were measured by IVIS-Lumina system 2 h after injection.

2.7. Tissue analysis

Collected tissues were processed by a homogenizer with cold lysis buffer and caspase-1 activity of the tissue lysate was measured using caspase-1 assay kit (Abcam, Cambridge, UK) in accordance with manufacturer's instruction. For histological analysis, colons were fixed in 4% formalin and embedded in paraffin. The paraffin-embedded samples were sectioned into 10 μm thick segments and stained with hematoxylin and eosin (H&E) and scored as previously described [26].

2.8. Statistical analysis

The data was analyzed using Graph Pad Prism 5.01 software (GraphPad Software, La Jolla, CA, USA). Statistical analysis was performed using two-tailed Student's *t*-test with 95% confidence interval or one-way analysis of variance (ANOVA) followed by Newman-Keuls *t*-test for comparisons of values among different groups. Data are expressed as the mean ± standard deviation. A p value of < 0.05 was considered statistically significant.

3. Results

3.1. Characterization of caspase-1-activatable fluorescent probe

Prior to the biological application of the synthetic Cas-1 probe, we examined its stability and cellular toxicity. UV–vis absorbance spectrophotometry in a caspase activation buffer revealed a unique plasmon resonance peak at 628 nm, whereas emission spectra showed that fluorescence over 700 nm (emission peak of Cy5.5: 710 nm) was barely detectable, indicating efficient quenching of emission fluorescence by BHQ-3 (Supplementary Figs. 2d and e). Fluorescence was recovered when the WEHD substrates were cleaved by caspase-1 (Fig. 1a and b, and Supplementary Fig. 3). Quantitative measurement of emission fluorescence in the 676–800 nm range of the Cas-1 probe showed linear increase of signal intensity up to 10 unit/ml of caspase-1, whereas there was no detectable increase in fluorescence signal from a Cas-3 probe (DEVD as substrate) in the presence of caspase-1. Specific reactivity of the synthetic probes was further confirmed by incubation with other caspases, including caspase-3, 8, 11, or specific caspase-1 inhibitor, Ac-YVAD-cmk (Fig. 1c). Time-dependent gradual increase of fluorescence intensity was observed only in the samples incubated with caspase-1 (2 unit/ml), ensuring the specificity of the synthetic probes. In addition, the signal intensities were reduced to baseline levels in the presence of a caspase-1 inhibitor. Cellular toxicity test using phagocytic cells, THP-1 and BMDM, revealed negligible cell death up to 100 μg/ml of the probes, indicating a clear biocompatibility within the probe concentration range (Supplementary Fig. 4a). We also evaluated the potential hemolytic activity of the Cas-1 probe (Supplementary Figs. 4b–d). The probe did not show any significant hemolytic activity up to 80 μM (equivalent to 180.0 μg/ml) as assessed by spectrophotometric measurement of released hemoglobin and by intact RBC counting. Furthermore, *in vivo* injection of the Cas-1 probe (100 μg in 100 μl of saline) did not cause significant changes in CBC in general (Supplementary Table 1). Even though there was a significant increase of platelet counts and slight increase of lymphocyte counts, they remained within normal range [27]. Therefore, this synthetic Cas-1 probe is biocompatible and could be used for *in vitro* and *in vivo* application without significant toxicity.

In order to investigate whether the synthetic probes could be triggered by endogenous inflammasome activated caspase-1 within cellular cytoplasm, THP-1 cells or BMDMs were pre-incubated with the Cas-1 probes and sequentially stimulated with exogenous LPS and ATP, well-known activators of cellular inflammasome (Fig. 1d and e). Cells treated with the inflammasome stimulators efficiently emitted Cy5.5-specific fluorescence within the cytoplasm, as measured by confocal fluorescent microscopy and flow cytometric analysis. These results indicated that the synthetic probes can penetrate cellular plasma membrane and are accessible to active caspase-1 within the cytoplasm. Activation of cellular inflammasome was indirectly confirmed by secretion of IL-1β into media in the stimulated phagocytic cells (Fig. 1f). In addition, activation of inflammasome was significantly inhibited in the presence of a caspase-1 inhibitor, as assessed by reduced fluorescence and IL-1β secretion from the stimulated phagocytic cells (Fig. 1d – f). Cells loaded with Cas-3 probe did not emit significant fluorescence after stimulation, indicating that signal emission by the Cas-1 probe upon inflammasome activation is specific (Fig. 1d and e).

3.2. In vivo imaging of caspase-1 activation in acute inflammatory disorders

Next, we examined whether Cas-1 probes could be applied to detect active caspase-1 *in vivo*. LPS and ATP solution containing 5 μg and 5 mg, respectively, in 50 μl of saline was injected into mice foot pads and the probes were intravenously delivered at the indicated time after injection of the stimulators. Then, *in vivo* fluorescence was non-invasively monitored by using IVIS-Lumina imaging system. When mice were injected with the probe at 2 h after LPS and ATP stimulation, fluorescence gradually intensified at foot pads and legs of the stimulated side, but not of the unstimulated side, up to 2 h after inducing the reaction with the (Supplementary Fig. 5a). At 2 h after injection of LPS and ATP, the probe was administered. Radiation efficiencies, as well as relative radiation, of the fluorescence of stimulated sites were significantly higher than those of unstimulated foot pads of the same mouse at 30 min after probe injection (Fig. 2a and b). The mean radiation efficiency of stimulated sites (mean ± S.D.: $2.0 \times 10^{10} \pm 2.2 \times 10^{9}$) was four times higher than that of unstimulated foot pads ($5.0 \times 10^{9} \pm 1.9 \times 10^{8}$) at 6 h after stimulation. *In vivo* fluorescence was barely detectable in the stimulated foot pads of caspase-1/11 KO mice (Fig. 2a), indicating that *in vivo* fluorescence is specifically generated by active caspase-1 via inflammasome activation. We confirmed significant increase of caspase-1 activity in tissue lysates of the stimulated foot pads of LPS/ATP-treated mice at 6 h after stimulation (Fig. 2c). Since mice were moribund immediately after injection with LPS and ATP, we measured the changes in rectal temperature as a systemic indicator of septic shock (Fig. 2d). Rectal temperatures of stimulated mice sharply decreased to ~30.5 °C (normal temp.: ~36.0 °C) by 1 h, but recovered to normal range at 1.5 h after LPS/ATP treatment. The stimulated mice fully recovered and were as active as unstimulated mice at 3 h after the

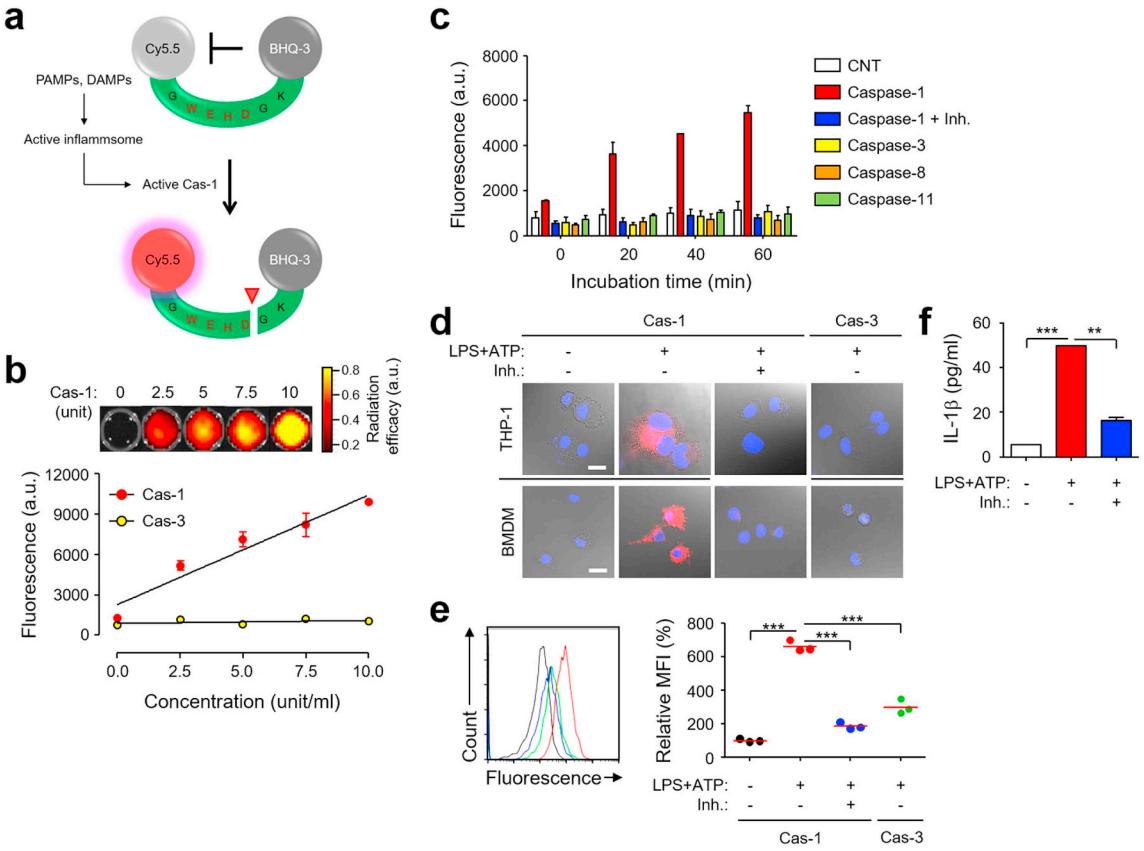

Fig. 1. *In vitro* characterization of the activatable Cas-1 fluorescence probe. (**a**) Diagram of Cas-1 probe design. (**b**) Relative fluorescence intensity emitted from the Cas-1 or Cas-3 probe (2 μg/ml) after incubation with the indicated concentrations of caspase-1 for 60 min at 37 °C. Upper, the corresponding NIR fluorescence images of the Cas-1 probe treated with various concentrations of caspase-1; lower, linear regression of relative fluorescence intensities from duplicated experiments. The excitation wavelength was fixed at 675 nm and emission wavelength was measured from 676 nm to 800 nm for detection of fluorescence radiation. Error bars: ± standard deviation (n = 3). (**c**) Kinetic changes of fluorescence intensities emitted from the Cas-1 probe (2 μg/ml) in the presence of various caspases (5 unit/ml of caspase-1, -3, -8, -11, and caspase-1 plus inhibitor) at the indicated incubation time. CNT, negative control without caspase. Cas: caspase, Inh: inhibitor. Error bars: + standard deviation (n = 3). (**d**) THP-1 cells and BMDMs were labeled with Cas-1 or Cas-3 probe (1.5 μg/ml) for 30 min, then, treated with LPS (1.5 μg/ml) for 3 h, followed by ATP (5 mM) for 30 min. Cells were fixed, labeled with DAPI for nuclear staining, and observed under a confocal microscope. Confocal microscopic images of unstimulated control (U.S.) and stimulated cells in the presence of caspase-1 inhibitor (LPS + ATP/Inh) are presented. Blue, nucleus; red, Cas-1 fluorescence. Bar, 20 μm. (**e**) Relative fluorescence intensities of THP-1 cells treated with LPS + ATP in the presence or absence of an inhibitor were assessed by flow cytometry. Relative mean fluorescence intensities (MFI) from three independent experiments are plotted on the right panel. The mean value is indicated by the red line. (**f**) Concentration of IL-1β in the cell culture supernatants was measured by ELISA after treating THP-1 cells with LPS ± ATP in the presence or absence of the inhibitor for 24 h. Error bars: + standard deviation (n = 2). (For interpretation of the references to colour in this figure legend, the reader is referred to the Web version of this article.)

stimulation. TNF-α and IL-6, inflammatory cytokines induced in systemic shock, in sera of stimulated mice were also significantly elevated at 2 h after LPS/ATP administration and declined to near the baseline by 6 h (Fig. 2e). IL-1β levels, a cytokine released upon inflammasome activation, in sera of stimulated mice were slightly, but significantly, increased from 6 h after stimulation, suggesting a minor role of IL-1β in symptomatic presentation during transient septic shock. Nevertheless, kinetic changes of IL-1β concentration in sera of stimulated mice were consistent with the fluorescence emission of the Cas-1 probe as measured by *in vivo* imaging, as well as caspase-1 activity, at the injection sites of LPS and ATP. Since we also observed a gradual and specific increase in fluorescence radiation along mice legs of the stimulated side, but not of the unstimulated side of the same mouse (Supplementary Fig. 5a), we suspected a lymphatic outflow of the activated fluorescent probes, generated at the stimulated foot pad by inflammasome activation, to the draining lymph nodes. Therefore, popliteal lymph nodes, draining lymph nodes of foot pad, were surgically collected and applied for *ex vivo* fluorescence imaging. As expected, we could consistently observe significantly elevated fluorescence in the draining lymph nodes, of the stimulated foot pads from 2 h after stimulation, when compared to those of non-stimulated foot pads from the same mice (Fig. 2f and g). *Ex vivo* fluorescence was barely detectable in neither stimulated nor non-stimulated draining lymph nodes in caspase-1/11 KO mice even at 6 h after stimulation (Fig. 2f), reinforcing the specificity of fluorescence emission by the Cas-1 probe via caspase-1 activation at the stimulated site. These results suggest that *in vivo* inflammasome activation by the exogenous stimulators can be efficiently and spatiotemporally monitored by the activatable Cas-1 probe during the acute phase of inflammation.

To further investigate the applicability of the synthetic probes as an imaging agent *in vivo*, we selected the DSS-induced IBD model, in which inflammasome activation plays a critical role in intestinal homeostasis [28]. *In vivo* fluorescence in abdomens of mice supplied with 3% DSS-containing water gradually increased up to 3 d after ingestion and significantly higher (~two fold) fluorescence radiation efficiencies (mean ± S.D.: $1.1 \times 10^{10} \pm 1.2 \times 10^{9}$) were detectable at 2 d after ingestion than those ($6.3 \times 10^{9} \pm 5.7 \times 10^{8}$) of unstimulated mice (Fig. 3a and b, and Supplementary Figs. 5b and 5c). Again, *in vivo* fluorescence was not significant in abdomens of caspase-1/11 KO mice up to 3 d of DSS administration. We observed significant weight loss, starting at 6 d after DSS ingestion (Fig. 3c), and shrinkage of large intestines from 2 d after DSS treatment (Fig. 3d and e). Interestingly,

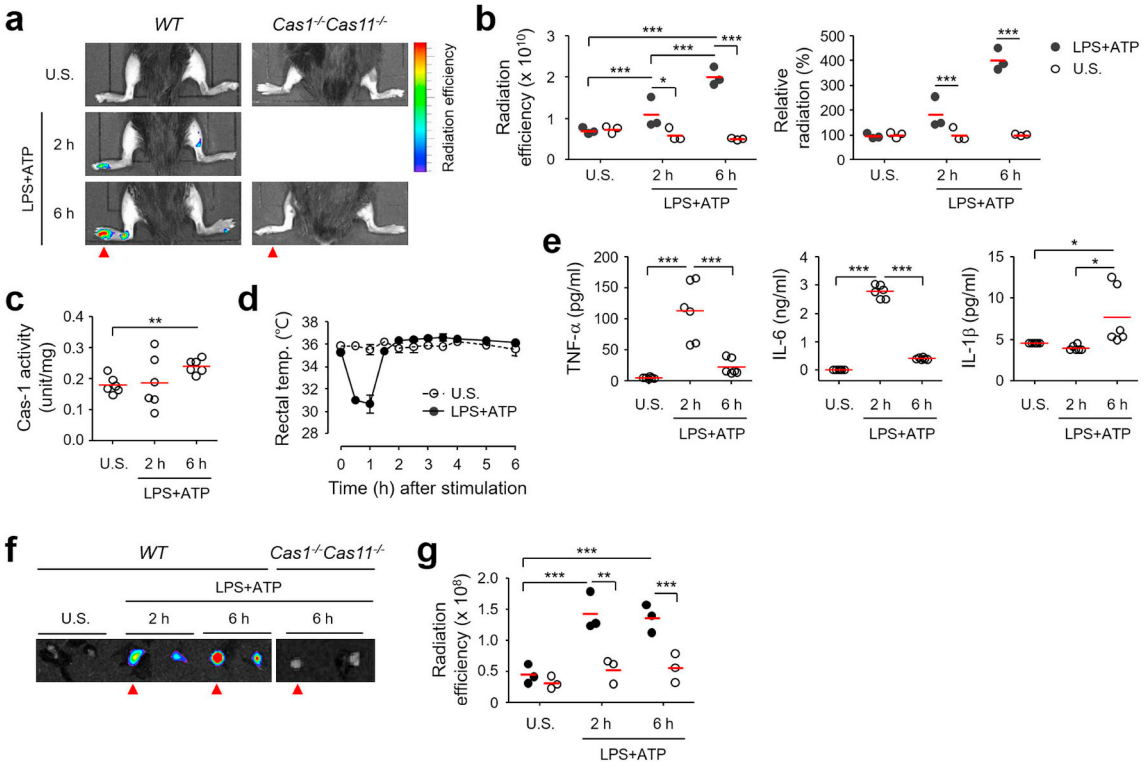

Fig. 2. *In vivo* imaging of caspase-1 activation after endotoxin stimulation. (**a**) LPS/ATP solution (5 μg and 5 mg/mouse, respectively) was injected into the indicated foot pads (red arrowhead) of mice and the Cas-1 probes were intravenously delivered at the indicated time after LPS/ATP injection. Then, *in vivo* fluorescence in legs of mice were monitored at 30 min after the probe injection using IVIS-Lumina imaging system. (**b**) Comparison of fluorescence radiation in the right food pads (black circles) stimulated with LPS/ATP with those of unstimulated sides (open circles) at the indicated time after stimulation ($n = 3$). Absolute counts of radiation efficiencies (left panel) and relative radiation (right panel) of the stimulated sites, normalized to unstimulated ones, are presented. Red line: mean. (**c**) Tissue lysates from foot pads stimulated with LPS/ATP were analyzed by caspase-1 activity kit at the indicated time after stimulation ($n = 6$). (**d**) Kinetic changes of rectal temperature of mice injected with LPS/ATP at the foot pads ($n = 3$). Error bar: ± S.D. (**e**) Concentration of inflammatory cytokines (IL-1β, IL-6, and TNF-α) were measured in sera of mice stimulated with LPS/ATP at the foot pads ($n = 3$, duplicated). (**f**) Representative images of fluorescence radiation in popliteal lymph nodes from mice stimulated with LPS/ATP at the foot pads. A pair of lymph nodes, one from stimulated leg (red arrowhead) and the other from unstimulated side, were simultaneously analyzed at the indicated time after stimulation. (**g**) Quantitation of fluorescence intensities in (**f**) ($n = 3$). U.S., unstimulated. *, $p < 0.05$; **, $p < 0.01$; ***, $p < 0.001$. (For interpretation of the references to colour in this figure legend, the reader is referred to the Web version of this article.)

elevated fluorescence intensity was initially prominent on the large intestines in the ascending colon near the cecum and the rectum edge of the descending colon, and then, gradually disseminated to transverse parts (Fig. 3d). When we analyzed the histological changes in the stimulated colon up to 3 d of DSS treatment, tissues from more fluorescent sites presented pathological changes with mild epithelial erosions and crypt atrophy, earlier than those from areas with lower radiation efficiencies (Fig. 3f and g); however, the histopathological grades were generally mild (histopathological scores: 1 out of 12) [26]. This suggests a potential correlation of pathological changes with the degree of inflammasome activation during the early stage of colonial inflammation. Gradual increase of fluorescence intensities was also observed in intestine-draining mesenteric lymph nodes *ex vivo* during the acute phase of inflammatory bowel disease (Fig. 3h).

3.3. In vivo imaging of caspase-1 activation in tumors and Alzheimer's disease model

Since the role of inflammasome in various chronic inflammatory disorders has recently been established [8,10,29], we next investigated the potential association of caspase-1 activation with initiation and progression of cancers and AD in mice models. First, we subcutaneously injected MC38 colon cancer cells into nude mice and performed *in vivo* imaging of caspase-1 activation using the Cas-1 probes. As shown in Fig. 4a–c, fluorescence intensities and radiation areas gradually increased at the injection sites, as the tumors grew. The tumor volumes were generally correlated with the radiation efficiency of fluorescence (Fig. 4b) and significant rise of fluorescence intensities at the tumor injection sites were detectable from 5 d after implantation (Fig. 4c). Gradual elevation of fluorescence in tumor-draining inguinal lymph nodes was also observed in *ex vivo* imaging analysis and the radiation efficiencies were significantly higher at 15 d after tumor injection when the average tumor volume reached approximately 300 mm^3 (Fig. 4d and e). Interestingly, we also observed significant increase of fluorescence intensities in non-draining popliteal lymph nodes at 15 d after tumor injection, suggesting a systemic increase of inflammasome activity in distal lymph nodes (Fig. 4d and e, right panels). We also traced inflammasome activation in a metastatic cancer model using the Cas-1 probe. Athymic nude mice were intravenously injected with MC38 cancer cells, resulting in pulmonary metastases of the cancer cells [30] (Fig. 4f and g). Non-invasive *in vivo* imaging of upper backs of mice by eXplore Optix system showed a gradual increase of fluorescence in four out of five mice at 15–20 d after injection with MC38 cells, although the differences in radiation efficiencies were not statistically different between the experimental groups (Fig. 4 f and g, upper panels). Nevertheless, we could observe multiple tumor nodules in all the mice at 20 d MC38 cell injection with. *Ex vivo* imaging of lungs with metastatic tumors after Cas-1 probe administration clearly showed gradual rise of fluorescence intensities throughout the lung tissues with significantly higher radiation at 20 d after tumor injection (Fig. 4f and g, lower panels).

Next, we investigated the potential association of caspase-1 activation with the initiation and progression of AD in mouse models [10]. T-

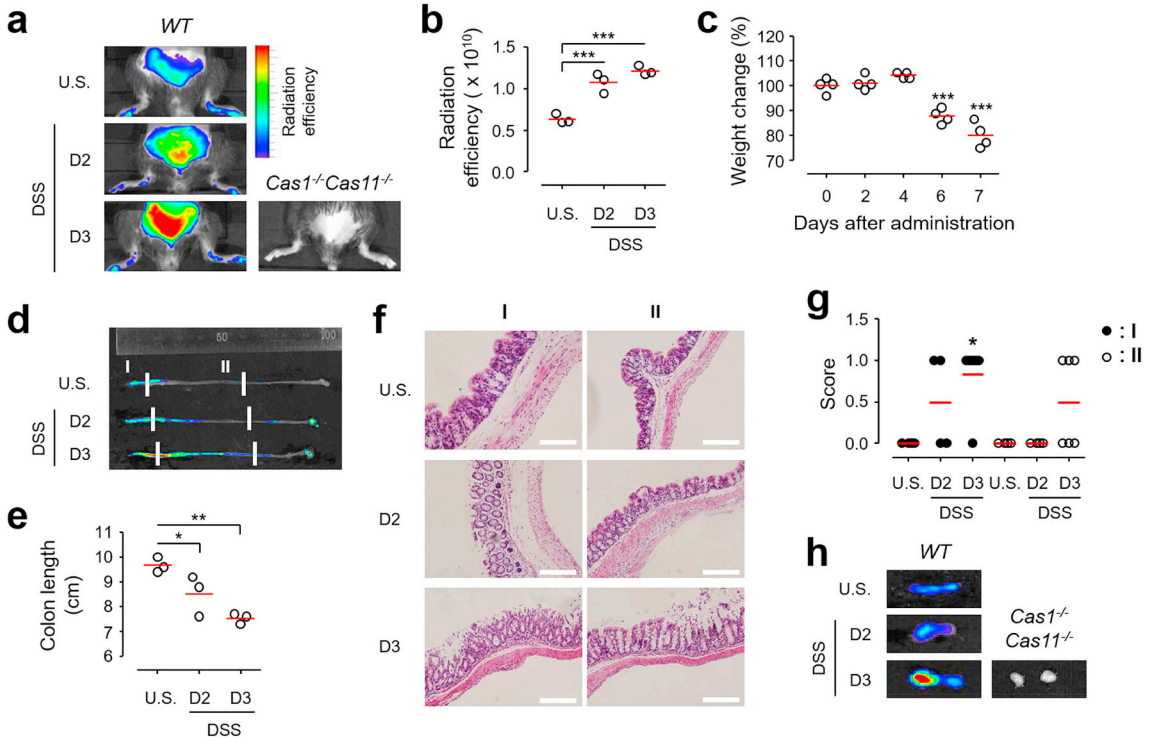

Fig. 3. *In vivo* imaging of caspase-1 activation in inflammatory bowel disease model. (**a**) Mice ingested water containing 3% DSS *ad libitum* and the Cas-1 probes were intravenously delivered at the indicated time (D2: day 2, D3: day 3). Then, *in vivo* fluorescence in the abdomens of mice was monitored by IVIS-Lumina imaging system. (**b**) Comparison of fluorescence radiation in abdomens of mice fed with 3% DSS water at the indicated time after stimulation ($n = 3$). Red line: mean. (**c**) Kinetic changes of body weight in mice at the indicated days after administration of 3% DSS water ($n = 4$). (**d**) Representative images of fluorescence radiation in colons from mice fed with 3% DSS water. White lines indicate the site of cross-section for histopathological analysis. (**e**) Kinetic changes of colon lengths collected from mice at the indicated days after administration of 3% DSS water ($n = 3$). (**f**) Representative histological images (hematoxylin and eosin staining) of tissue sections from sites I and II of colons indicated in (**d**). White bar, 200 μm. (**g**) Histopathological scores of site I (black circles) and II (open circles) of colon sections from mice fed with 3% DSS water ($n = 4$–6). (**h**) Representative images of fluorescence radiation in mesenteric lymph nodes from mice administered 3% DSS water. U.S., unstimulated. *, $p < 0.05$; **, $p < 0.01$; ***, $p < 0.001$. (For interpretation of the references to colour in this figure legend, the reader is referred to the Web version of this article.)

maze and Y-maze tests were performed to evaluate working memory and hippocampal-dependent spatial memory, respectively, in 2 to 5-month-old wild type (WT) and 5XFAD mice (Fig. 5a). The spontaneous alternation ratio observed in the T-maze and Y-maze tests were not significantly different between WT and 5xFAD mice at 3–4 months of age, as previously reported [31]. However, alternation ratios decreased in 5-month-old 5xFAD mice when compared with WT, indicating significant cognitive impairments from 5 months in 5xFAD mice. Caspase-1 activity in the hippocampus was also significantly increased at 5–6 months of age in 5xFAD mice, as measured by a commercially available caspase-1 enzyme assay kit of tissue lysates (Fig. 5b). These results suggest that increased caspase-1 activity is dependent on age and is correlated with cognitive impairments in AD mice. Next, we examined caspase-1 activation in AD mouse model by *in vivo* imaging after intravenous injection of the Cas-1 probe. Fluorescence intensities on tops of heads of 5xFAD mice gradually increased in an age-dependent manner when compared to those of WT mice (Fig. 5c). Surprisingly, we found a significant increase of fluorescence intensities from 3-month-old 5xFAD mice, when cognitive impairments were not yet present. E*x vivo* imaging consistently showed that caspase-1 activation in the brains of 5xFAD mice was significantly elevated from 3-month old 5xFAD mice, although fluorescence radiation also gradually increased in WT mice in an age-dependent manner (Fig. 5d, right upper panel). Relative radiation from the brains of 5xFAD mice at 3-months of old age was approximately 50% higher than those of WT mice of the same age (Fig. 5d, right lower panel). Notably, the strong fluorescence intensities were observed in central parts of the brain (Fig. 5d), as previously reported [22]. Since we observed a gradual increase of fluorescence in the brains of WT mice, we suspected diffusion of the probe, potentially due to breakdown of the BBB in the brain as mice age [32]. In order to determine whether diffusion of the florescent probe through the BBB in the brain increases in an age-dependent manner, we examined *ex vivo* fluorescence radiation of brains from WT and 5xFAD mice at 3-month and 6-month-old age after intravenous injection of Cy5.5-conjugated peptide only (without a quencher). As shown in Fig. 5e and f, although the radiation efficiency was higher in 6-month-old mice than 3-month-old mice, the difference of fluorescence radiation was not significant between the brains of 3 and 6-month-old WT and 5xFAD mice. These findings indicate that caspase-1 is activated before cognitive impairment in 5xFAD mice, although baseline diffusion of the synthetic probe into brain tissues through the BBB also increases as mice age, as previously reported [32].

Recently, it has also been reported that there is lymphatic outflow in the brain into superficial cervical lymph nodes through deep cervical lymph nodes located in the neck [33–35]. Since we observed consistent caspase-1 activation in draining lymph nodes of inflammatory sites, we speculated that activation of caspase-1 in AD model flows to brain-draining lymph nodes in the necks of 5xFAD mice. To confirm cerebrospinal fluid (CSF) flow routes to draining lymph nodes, we anesthetized mice and intracerebroventricularly injected a mixture of Evans blue and free Cy5.5 fluorescent dye, and then imaged mandibular and deep cervical lymph nodes in the neck at 15, 30, and 60 min after injection (Supplementary Fig. 6). Deep cervical lymph nodes were stained with Evans blue and had fluorescent signal at 15 min after dye injection and the signals steadily increased over time. The mandibular lymph nodes had slightly delayed dynamics, the fluorescence signal within the nodes was detected in all mice at 30 min after injection. A

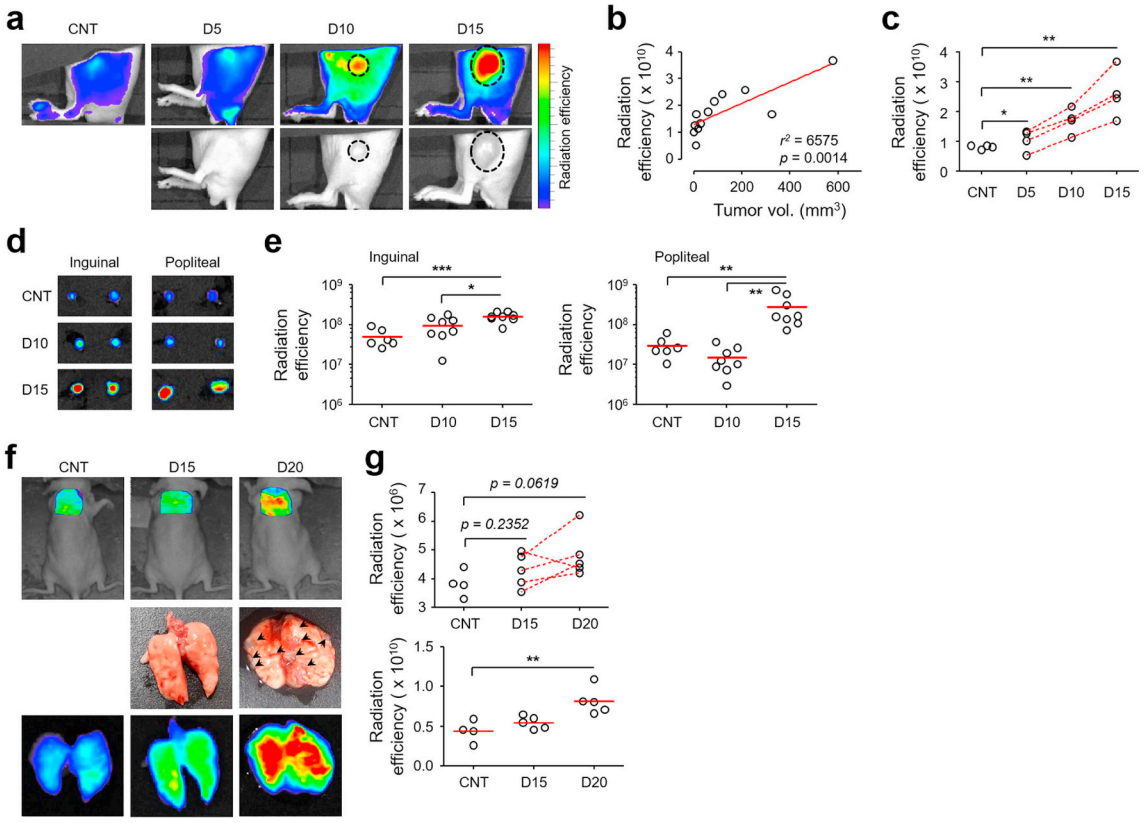

Fig. 4. *In vivo* imaging of caspase-1 activation in cancer model. (**a**) MC38 colon cancer cells (5×10^6 cells/mouse) were subcutaneously injected into the flank of athymic nude mice and the Cas-1 probe was intravenously delivered at the indicated days after cancer cell injection. Then, *in vivo* fluorescence at tumor injection sites of mice was monitored by using IVIS-Lumina imaging system. (**b**) Correlation of radiation efficiency with tumor volume at the injection sites. (**c**) Kinetic changes of fluorescence intensities at the sites of tumors at the indicated time after cancer cell injection ($n = 4$). (**d**) Representative images of fluorescence radiation in tumor-draining inguinal lymph nodes and non-draining popliteal lymph nodes at the indicated time after cancer cell injection. (**e**) Radiation efficiencies of fluorescence emitted from lymph nodes in (**d**) ($n = 6$–8). Red line: mean. (**f**) Athymic nude mice were intravenously injected with MC38 cells (5×10^5 cells/mouse) via the lateral tail vein and the Cas-1 probes were intravenously delivered at the indicated days after cancer cell injection. Then, fluorescence radiation of the upper backs (top panels) or *ex vivo* lungs (middle and bottom panels) of mice was monitored by eXplore Optix system or IVIS-Lumina imaging system, respectively. (**g**) Radiation efficiencies of fluorescence emitted from upper backs (top panel) or *ex vivo* lungs (bottom panel) in (**f**) ($n = 4$–5). CNT, normal mouse control. *, $p < 0.05$; **, $p < 0.01$; ***, $p < 0.001$. (For interpretation of the references to colour in this figure legend, the reader is referred to the Web version of this article.)

significant increase of fluorescence intensities at the lymph node sites in the neck was observed even by non-invasive *in vivo* imaging of fluorescent dyes up to 60 min after injection, suggesting rapid and sustained lymphatic outflow of CSF to draining lymph nodes (Supplemented Fig. 6a), as previously reported [35,36]. Therefore, we assessed whether fluorescence radiation in the neck of 5xFAD mice increases by non-invasive imaging after injecting the Cas-1 probe. Indeed, we observed significantly enhanced radiation in 5xFAD mice from four-months of age, when compared to that of WT mice (Fig. 6a and c). We also confirmed that fluorescence intensities in deep cervical and superficial cervical lymph nodes *ex vivo* gradually elevated over time in 5xFAD mice (Fig. 6b and c). It is notable the relative fluorescence radiation was significantly higher in superficial cervical lymph nodes from three-months of age when compared to that of WT mice, whereas fluorescence intensities were significantly elevated in deep cervical lymph nodes only at six-month age in AD model mice. Nevertheless, these results indicate that non-invasive imaging of fluorescence radiation from Cas-1 probes can be used to detect lymphatic outflow from inflamed brain lesions to the necks of 5xFAD mice as an indirect measurement of brain inflammation (i.e. the activation of inflammasome).

4. Discussion

Recent advances in the use of "activatable" fluorescence probes in optical imaging have demonstrated their wide applicability in *in vitro* and *in vivo* monitoring of various biological activities and have facilitated biomedical applications in pre-clinical and clinical settings for drug discovery, diagnosis, and therapeutic monitoring [37,38]. Activatable fluorescence probes comprise of a fluorophore and quencher connected by a molecular linker which responds to specific biochemical alterations and/or abnormalities. The activated probes then generate an amplified fluorescence signal when the physical distance between the fluorophore and quencher molecules increases *in situ* at the target site in a live organism [37]. In previous studies, we and others have successfully developed activatable fluorescent probes that respond to diverse biological enzymes, including cathepsins, matrix metalloproteases, thrombin, and caspases, to target and monitor cancers, arthritis, and ischemic lesions associated with that specific enzyme activity by non-invasive *in vivo* imaging analysis [38–41].

Despite our expanding understanding of the biological significance of inflammasome in various acute and chronic disorders, current technologies to detect inflammasome activity have practical limitations for *in vivo* application. Tools for monitoring inflammasome activation have primarily relied on indirect and *in vitro* methods measuring the levels of IL-1β or IL-18 secreted from inflamed cells or tissues [18]. Direct monitoring of caspase-1 activity, a hallmark executor of various inflammasome machinery, generally requires cellular lysis during biochemical analysis [18] or genetic modification of target cells for *in vitro* or *in vivo* application [42,43]. All the recent technologies directly detecting *in vivo* speck formation by ASC complexes upon inflammasome

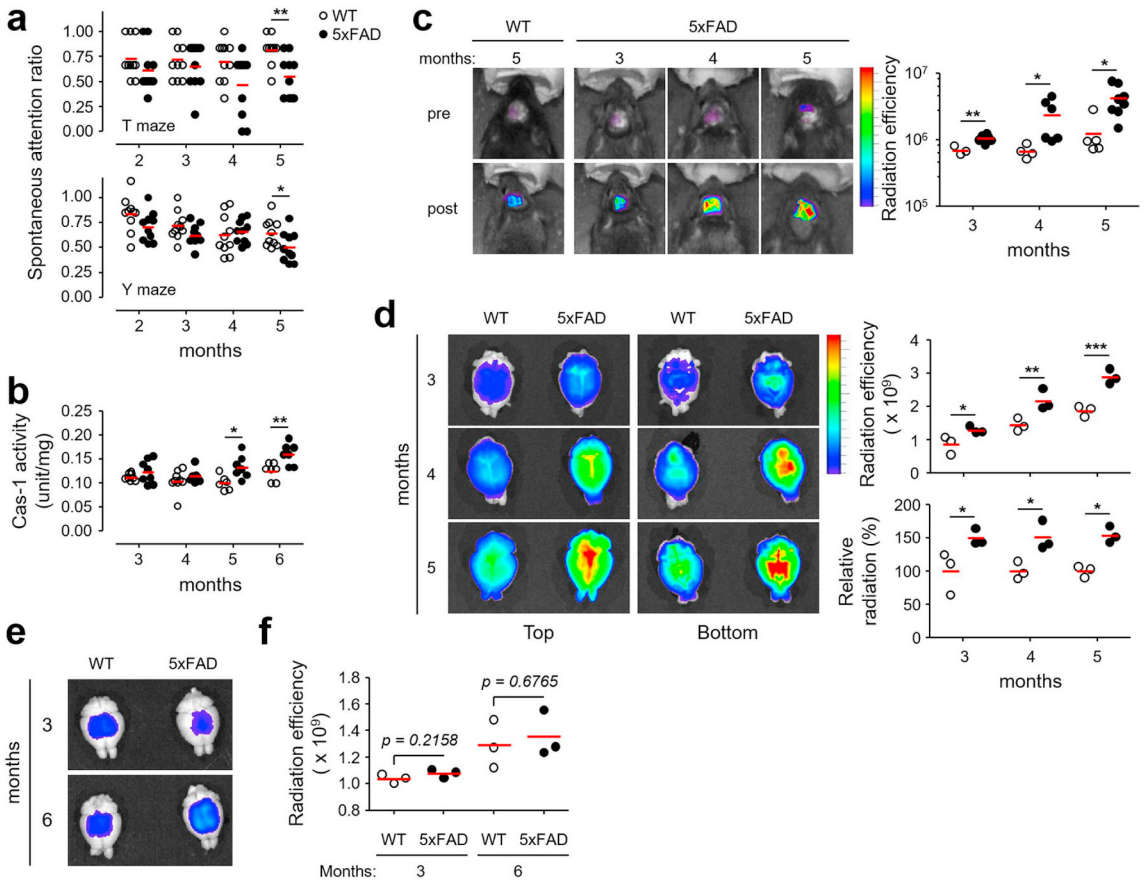

Fig. 5. *In vivo* imaging of caspase-1 activation in Alzheimer's disease model. (**a**) WT (open circles) and 5xFAD (black circles) mice at the indicated months of age were tested for working memory (T-maze task, top panel) and hippocampal-dependent spatial memory (Y-maze task, bottom panel) (n = 10/group). Red line: mean. (**b**) Tissue lysates of hippocampi from mice at the indicated months of age were analyzed by caspase-1 activity kit (n = 6–9/group). Open circles, WT; black circles, 5xFAD mice. (**c**) Fluorescence radiation from heads of WT (open circles) or 5xFAD (black circles) mice at the indicated months of age was analyzed by eXplore Optix system after Cas-1 probe intravenous injection. Representative fluorescence images of tops of mice heads (left panels) and quantitative comparison of total photons per unit area (right panel) at the indicated age are presented. (**d**) Fluorescence efficiencies of brains collected from WT or 5xFAD mice at the indicated months of age were analyzed by IVIS-Lumina imaging system after Cas-1 probe intravenous injection. Representative fluorescence images (left panels) of *ex vivo* brains collected from mice at the indicated months of age, absolute counts of radiation efficiencies (right top panel), and relative radiation normalized to those of WT mice of the same age (right panel) are presented. (**e** and **f**) Fluorescence efficiency of probes in brains collected from mice at the indicated age was analyzed by IVIS-Lumina imaging system after intravenous injection with Cy5.5-peptide conjugate without BHQ quencher (n = 3/group). *, $p < 0.05$; **, $p < 0.01$; ***, $p < 0.001$. (For interpretation of the references to colour in this figure legend, the reader is referred to the Web version of this article.)

activation in a cellular level also require genetic modification of the encoding gene [15–17]. In addition, methods using genetically modified ASC for speck formation as an inflammasome marker is intrinsically flawed due to the risk of non-specific aggregation without an inflammatory stimulus if overexpressed [17] as well as potentially adversely affecting the efficiency of caspase-1 activation via reduced recruitment of caspase-1 [16]. Moreover, detection of speck formation within cells or tissues upon stimulation requires knowing the exact site of inflammation or scanning the inflamed areas of stimulated tissues to identify cells containing ACS specks via microscopic imaging analysis. Therefore, all the currently available technologies have substantial limitations for direct *in vivo* imaging of intact organisms or tissues in a spatiotemporal way.

In this study, we developed a synthetic probe, which emits fluorescence radiation upon activation of caspase-1 within cells or tissues. Application of this novel probe for *in vivo* imaging of inflammasome activation provides several advantages over other technologies. First, the probe can penetrate cellular plasma membranes and readily access cellular cytoplasms, thereby emitting NIR fluorescence upon cleavage by active caspase-1 through inflammasome activation, as confirmed by confocal microscopy and flow cytometry (Fig. 1d and e). Enhanced membrane permeability of the peptide-based probe is possibly endowed by covalent conjugation of hydrophobic quencher [44]. Although we did not perform solubility test of the probe, we could assume relative hydrophobicity of the probe based on RP-HPLC analysis using hydrophobic acetonitrile gradient (5% → 95%) as a mobile solvent (Supplementary Fig. 2b). The probe was eluted at ~23 min when the solvent composition was 86% acetonitrile and 14% DW (including 0.1% TFA), suggesting relative hydrophobicity. Since the probe contains a peptide bridge comprised of four charged amino acids (Glu [E], His [H], Asp [D], and Lys [K]), it may have some amphipathic characteristics. This intrinsic property enables non-invasive *in vivo* imaging of fluorescence radiation from deep tissues, including the brain after penetration through the BBB, of a living organism. We observed gradual and significant increase of *in vivo* fluorescence around areas where a pathogenic insult was introduced in various inflammatory disease models, including cancer and AD. In addition, the specific signal emission was rapidly detectable from 30 min after intravenous probe administration and gradually rose up to 2 h of probe injection (Supplementary Fig. 5), thereby increasing signal to noise ratio. Second, the radiation efficiency and the fluorescence-emitting area of the activated Cas-1 probe correlate well with the degree of caspase-1 activity as measured by *in vitro, ex vivo,* and *in vivo* imaging assays. This probe also allows us to specify the inflamed site and the degree of inflammation in an organism and/or

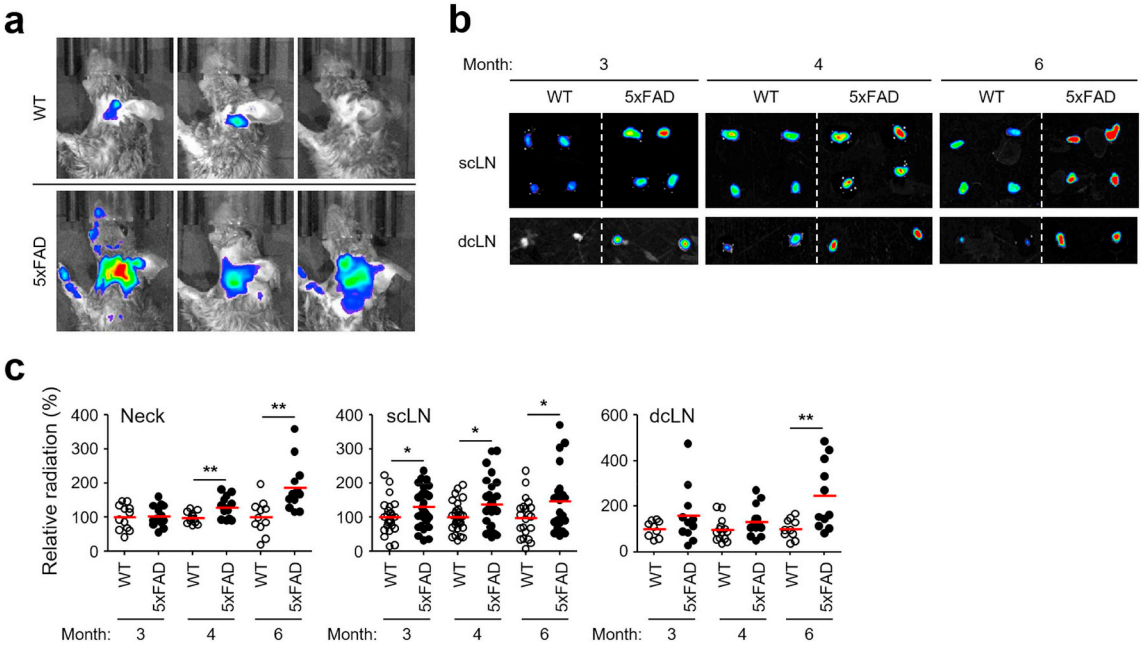

Fig. 6. *In vivo* imaging of caspase-1 activation in neck of Alzheimer's disease model. (**a**) Representative fluorescence image of necks of WT and 5xFAD mice at four-months of age. Mice were intravenously injected with the Cas-1 probe and monitored by IVIS-Lumina imaging system. (**b**) Representative images of fluorescence radiation in superficial (scLN) and deep cervical (dcLN) lymph nodes collected from mice at the indicated months of age. Mice were injected with Cas-1 probe at 2 h before lymph node collection. Red line: mean. (**c**) Quantitative comparison of relative fluorescence radiation from necks, scLNs, and dcLNs of 5xFAD mice after normalization with those of WT mice of the same age was performed using the data from (**b**). Neck, n = 11–14/group; scLN, n = 21–30/group; dcLN, 11–14/group. *, $p < 0.05$; **, $p < 0.01$. (For interpretation of the references to colour in this figure legend, the reader is referred to the Web version of this article.)

tissue by microscopic imaging analysis. For example, *ex vivo* imaging of colons in mice fed with DSS can specifically identify the inflammatory regions in which the histopathologic changes were more advanced even in the early stage of inflammatory bowel condition, as assessed by fluorescence intensities, (Fig. 3d ~ g). The intensities and area of fluorescence radiation can also help indirectly infer the size and distribution of cancer nodules (Fig. 4) and pathogenic inflammation in the brain that are possible sites of amyloid plaque deposition in the deep cortex, subiculum, and hippocampus during the early stage of AD pathogenesis (Fig. 5) [22]. Furthermore, the fluorescent probe can also label draining lymph nodes of inflamed sites, potentially via lymphatic outflow of free fluorescence probes or probe-associated cellular entities formed by pyroptosis. This property of Cas-1 probe could contribute to enhanced fluorescence by retaining the fluorescent probes near the inflammatory site and assist to localize the original source of inflammatory site by non-invasive *in vivo* imaging of draining lymph nodes, as we observed in various inflammatory conditions including AD (Fig. 6). Third, the synthetic probe is biocompatible and barely toxic to the cells as confirmed by cytotoxicity test and hemolytic activity assay. It did not significantly affect cellular viability up to 100 μg/ml and did not show hemolytic activity up to 180.0 μg/ml (Supplementary Fig. 4). Moreover, intravenous injection of the probe (100 μg) in mice did not cause significant hematological changes (Supplementary Table 1). The Cas-1 probe is likely rapidly secreted out through the kidney within a few hours after intravenous administration. Among the major organs of normal mice including liver, lung, spleen, and heart, we observed strong fluorescence radiation only in the kidney at 3 h after probe injection, which disappeared at 24 and 72 h (Supplementary Fig. 7). Low cellular toxicity and quick elimination within a live organism confer significant benefit for *in vivo* pre-clinical and clinical application.

In summary, we developed an activatable fluorescence probe that specifically responds to caspase-1 activity, a hallmark executor of inflammasome activation. This novel caspase-1 probe is efficiently delivered into cells and specifically emits fluorescence upon caspase-1 activation in *in vitro* and *in vivo* inflammatory conditions. Non-invasive *in vivo* imaging of caspase-1 activation enabled us to detect early stage of various inflammatory conditions that are initiated by inflammasome before symptomatic presentations. Particularly, *in vivo* inflammation of intestine in IBD model or brain in AD model is detected 4 d and 2 months earlier, respectively, before symptomatic signs. In addition, efficient visualization of inflammasome activity made it possible to pinpoint inflammatory sites where the associated pathologic changes occur. Therefore, efficient and rapid detection of caspase-1 activity *in vivo* can revolutionize the current paradigm for diagnosis and therapeutics in various inflammatory disorders associated with inflammasome activation.

Declaration of competing interest

The authors declare no competing interests.

Acknowledgments

This study was supported by the Intramural Research Program and the KU-KIST project of KIST, the Intramural Research Program of KIST, South Korea (2E29370), and by a grant (2017M3A9E4061998) of the National Research Foundation of Korea, South Korea (NRF) funded by the Korean government. This study was also partly supported by Seoul National University Bundang Hospital Research Fund, South Korea (02-2018-005). J.W.L., E.J.Y., and N.J. received a scholarship from the BK21-plus education program provided by the National Research Foundation of Korea.

Appendix A. Supplementary data

Supplementary data to this article can be found online at https://doi.org/10.1016/j.biomaterials.2019.119543.

Additional information

Supplementary information is available for this paper at.

Data availability

The authors declare that the data supporting the findings of this study are available within the paper and the supplementary information, or from the corresponding authors upon request. Relevant accession codes are provided within the specific Methods sections.

References

[1] F. Martinon, K. Burns, J. Tschopp, The inflammasome: a molecular platform triggering activation of inflammatory caspases and processing of proIL-beta, Mol. Cell 10 (2) (2002) 417–426.

[2] B.T. Cookson, M.A. Brennan, Pro-inflammatory programmed cell death, Trends Microbiol. 9 (3) (2001) 113–114.

[3] D. Sharma, T.D. Kanneganti, The cell biology of inflammasomes: mechanisms of inflammasome activation and regulation, J. Cell Biol. 213 (6) (2016) 617–629.

[4] S.M. Man, T.D. Kanneganti, Converging roles of caspases in inflammasome activation, cell death and innate immunity, Nat. Rev. Immunol. 16 (1) (2016) 7–21.

[5] Y.S. Yi, Regulatory roles of the caspase-11 non-canonical inflammasome in inflammatory diseases, Immune Netw. 18 (6) (2018).

[6] E. Latz, T.S. Xiao, A. Stutz, Activation and regulation of the inflammasomes, Nat. Rev. Immunol. 13 (6) (2013) 397–411.

[7] P. Broz, V.M. Dixit, Inflammasomes: mechanism of assembly, regulation and signalling, Nat. Rev. Immunol. 16 (7) (2016) 407–420.

[8] H. Guo, J.B. Callaway, J.P. Ting, Inflammasomes: mechanism of action, role in disease, and therapeutics, Nat. Med. 21 (7) (2015) 677–687.

[9] R. Karki, S.M. Man, T.D. Kanneganti, Inflammasomes and cancer, Cancer Immunol Res. 5 (2) (2017) 94–99.

[10] C. Venegas, S. Kumar, B.S. Franklin, T. Dierkes, R. Brinkschulte, D. Tejera, A. Vieira-Saecker, S. Schwartz, F. Santarelli, M.P. Kummer, A. Griep, E. Gelpi, M. Beilharz, D. Riedel, D.T. Golenbock, M. Geyer, J. Walter, E. Latz, M.T. Heneka, Microglia-derived ASC specks cross-seed amyloid-beta in Alzheimer's disease, Nature 552 (7685) (2017) 355–361.

[11] J.J. Kim, E.K. Jo, NLRP3 inflammasome and host protection against bacterial infection, J. Korean Med. Sci. 28 (10) (2013) 1415–1423.

[12] L. Franchi, T. Eigenbrod, R. Munoz-Planillo, G. Nunez, The inflammasome: a caspase-1-activation platform that regulates immune responses and disease pathogenesis, Nat. Immunol. 10 (3) (2009) 241–247.

[13] B.A. McKenzie, M.K. Mamik, L.B. Saito, R. Boghozian, M.C. Monaco, E.O. Major, J.Q. Lu, W.G. Branton, C. Power, Caspase-1 inhibition prevents glial inflammasome activation and pyroptosis in models of multiple sclerosis, Proc. Natl. Acad. Sci. U. S. A. 115 (26) (2018) E6065–E6074.

[14] R. Stienstra, L.A. Joosten, T. Koenen, B. van Tits, J.A. van Diepen, S.A. van den Berg, P.C. Rensen, P.J. Voshol, G. Fantuzzi, A. Hijmans, S. Kersten, M. Muller, W.B. van den Berg, N. van Rooijen, M. Wabitsch, B.J. Kullberg, J.W. van der Meer, T. Kanneganti, C.J. Tack, M.G. Netea, The inflammasome-mediated caspase-1 activation controls adipocyte differentiation and insulin sensitivity, Cell Metabol. 12 (6) (2010) 593–605.

[15] P. Sagoo, Z. Garcia, B. Breart, F. LemaOtre, D. Michonneau, M.L. Albert, Y. Levy, P. Bousso, In vivo imaging of inflammasome activation reveals a subcapsular macrophage burst response that mobilizes innate and adaptive immunity, Nat. Med. 22 (1) (2016) 64–+.

[16] T.C. Tzeng, S. Schattgen, B. Monks, D. Wang, A. Cerny, E. Latz, K. Fitzgerald, D.T. Golenbock, A fluorescent reporter mouse for inflammasome assembly demonstrates an important role for cell-bound and free ASC specks during in vivo infection, Cell Rep. 16 (2) (2016) 571–582.

[17] P. Kuri, N.L. Schieber, T. Thumberger, J. Wittbrodt, Y. Schwab, M. Leptin, Dynamics of in vivo ASC speck formation, J. Cell Biol. 216 (9) (2017) 2891–2909.

[18] M. O'Brien, D. Moehring, R. Munoz-Planillo, G. Nunez, J. Callaway, J. Ting, M. Scurria, T. Ugo, L. Bernad, J. Cali, D. Lazar, A bioluminescent caspase-1 activity assay rapidly monitors inflammasome activation in cells, J. Immunol. Methods 447 (2017) 1–13.

[19] N.A. Thornberry, T.A. Rano, E.P. Peterson, D.M. Rasper, T. Timkey, M. Garcia-Calvo, V.M. Houtzager, P.A. Nordstrom, S. Roy, J.P. Vaillancourt, K.T. Chapman, D.W. Nicholson, A combinatorial approach defines specificities of members of the caspase family and granzyme B. Functional relationships established for key mediators of apoptosis, J. Biol. Chem. 272 (29) (1997) 17907–17911.

[20] S. Lee, K.Y. Choi, H. Chung, J.H. Ryu, A. Lee, H. Koo, I.C. Youn, J.H. Park, I.S. Kim, S.Y. Kim, X. Chen, S.Y. Jeong, I.C. Kwon, K. Kim, K. Choi, Real time, high resolution video imaging of apoptosis in single cells with a polymeric nanoprobe, Bioconjug. Chem. 22 (2) (2011) 125–131.

[21] T.C. Cheong, E.P. Shin, E.K. Kwon, J.H. Choi, K.K. Wang, P. Sharma, K.H. Choi, J.M. Lim, H.G. Kim, K. Oh, J.H. Jeon, I. So, I.G. Kim, M.S. Choi, Y.K. Kim, S.Y. Seong, Y.R. Kim, N.H. Cho, Functional manipulation of dendritic cells by photoswitchable generation of intracellular reactive oxygen species, ACS Chem. Biol. 10 (3) (2015) 757–765.

[22] H. Oakley, S.L. Cole, S. Logan, E. Maus, P. Shao, J. Craft, A. Guillozet-Bongaarts, M. Ohno, J. Disterhoft, L. Van Eldik, R. Berry, R. Vassar, Intraneuronal beta-amyloid aggregates, neurodegeneration, and neuron loss in transgenic mice with five familial Alzheimer's disease mutations: potential factors in amyloid plaque formation, J. Neurosci. 26 (40) (2006) 10129–10140.

[23] R.M. Deacon, J.N. Rawlins, T-maze alternation in the rodent, Nat. Protoc. 1 (1) (2006) 7–12.

[24] C.J. Miedel, J.M. Patton, A.N. Miedel, E.S. Miedel, J.M. Levenson, Assessment of spontaneous alternation, novel object recognition and limb clasping in transgenic mouse models of amyloid-beta and tau neuropathology, J. Vis. Exp. 123 (2017).

[25] M.K. Shim, H.Y. Yoon, J.H. Ryu, H. Koo, S. Lee, J.H. Park, J.H. Kim, S. Lee, M.G. Pomper, I.C. Kwon, K. Kim, Cathepsin B-specific metabolic precursor for in vivo tumor-specific fluorescence imaging, Angew Chem. Int. Ed. Engl. 55 (47) (2016) 14698–14703.

[26] B. Chassaing, J.D. Aitken, M. Malleshappa, M. Vijay-Kumar, Dextran sulfate sodium (DSS)-induced colitis in mice, Curr. Protoc. Im. 104 (2014) Unit 15 25.

[27] T. Fukuda, E. Asou, K. Nogi, K. Goto, Evaluation of mouse red blood cell and platelet counting with an automated hematology analyzer, J. Vet. Med. Sci. 79 (10) (2017) 1707–1711.

[28] M.H. Zaki, M. Lamkanfi, T.D. Kanneganti, The Nlrp3 inflammasome: contributions to intestinal homeostasis, Trends Immunol. 32 (4) (2011) 171–179.

[29] Q. He, Y. Fu, D. Tian, W. Yan, The contrasting roles of inflammasomes in cancer, Am. J. Cancer Res. 8 (4) (2018) 566–583.

[30] R. Zaynagetdinov, T.P. Sherrill, L.A. Gleaves, A.G. McLoed, J.A. Saxon, A.C. Habermann, L. Connelly, D. Dulek, R.S. Peebles Jr., B. Fingleton, F.E. Yull, G.T. Stathopoulos, T.S. Blackwell, Interleukin-5 facilitates lung metastasis by modulating the immune microenvironment, Cancer Res. 75 (8) (2015) 1624–1634.

[31] L. Devi, M. Ohno, TrkB reduction exacerbates Alzheimer's disease-like signaling aberrations and memory deficits without affecting beta-amyloidosis in 5XFAD mice, Transl. Psychiatry 5 (2015) e562.

[32] A. Montagne, S.R. Barnes, M.D. Sweeney, M.R. Halliday, A.P. Sagare, Z. Zhao, A.W. Toga, R.E. Jacobs, C.Y. Liu, L. Amezcua, M.G. Harrington, H.C. Chui, M. Law, B.V. Zlokovic, Blood-brain barrier breakdown in the aging human hippocampus, Neuron 85 (2) (2015) 296–302.

[33] S. Da Mesquita, A. Louveau, A. Vaccari, I. Smirnov, R.C. Cornelison, K.M. Kingsmore, C. Contarino, S. Onengut-Gumuscu, E. Farber, D. Raper, K.E. Viar, R.D. Powell, W. Baker, N. Dabhi, R. Bai, R. Cao, S. Hu, S.S. Rich, J.M. Munson, M.B. Lopes, C.C. Overall, S.T. Acton, J. Kipnis, Functional aspects of meningeal lymphatics in ageing and Alzheimer's disease, Nature 560 (7717) (2018) 185–191.

[34] A. Louveau, I. Smirnov, T.J. Keyes, J.D. Eccles, S.J. Rouhani, J.D. Peske, N.C. Derecki, D. Castle, J.W. Mandell, K.S. Lee, T.H. Harris, J. Kipnis, Structural and functional features of central nervous system lymphatic vessels, Nature 523 (7560) (2015) 337–341.

[35] Q.L. Ma, B.V. Ineichen, M. Detmar, S.T. Proulx, Outflow of cerebrospinal fluid is predominantly through lymphatic vessels and is reduced in aged mice, Nat. Commun. 8 (2017).

[36] W. Van den Broeck, A. Derore, P. Simoens, Anatomy and nomenclature of murine lymph nodes: descriptive study and nomenclatory standardization in BALB/cAnNCrl mice, J. Immunol. Methods 312 (1–2) (2006) 12–19.

[37] S. Lee, K. Park, K. Kim, K. Choi, I.C. Kwon, Activatable imaging probes with amplified fluorescent signals, Chem. Commun. 36 (2008) 4250–4260.

[38] B.M. Luby, D.M. Charron, C.M. MacLaughlin, G. Zheng, Activatable fluorescence: from small molecule to nanoparticle, Adv. Drug Deliv. Rev. 113 (2017) 97–121.

[39] K. Kim, M. Lee, H. Park, J.H. Kim, S. Kim, H. Chung, K. Choi, I.S. Kim, B.L. Seong, I.C. Kwon, Cell-permeable and biocompatible polymeric nanoparticles for apoptosis imaging, J. Am. Chem. Soc. 128 (11) (2006) 3490–3491.

[40] J.H. Ryu, A. Lee, J.U. Chu, H. Koo, C.Y. Ko, H.S. Kim, S.Y. Yoon, B.S. Kim, K. Choi, I.C. Kwon, K. Kim, I. Youn, Early diagnosis of arthritis in mice with collagen-induced arthritis, using a fluorogenic matrix metalloproteinase 3-specific polymeric probe, Arthritis Rheum. Us 63 (12) (2011) 3824–3832.

[41] S. Park, J. Lee, M.H. Jo, J.H. Na, S.G. Park, H.K. Jang, S.W. Kang, J.H. Kim, B.S. Kim, J.H. Park, I.C. Kwon, J.H. Ryu, K. Kim, In vivo monitoring of angiogenesis in a mouse hindlimb ischemia model using fluorescent peptide-based probes, Amino Acids 48 (7) (2016) 1641–1654.

[42] T. Liu, Y. Yamaguchi, Y. Shirasaki, K. Shikada, M. Yamagishi, K. Hoshino, T. Kaisho, K. Takemoto, T. Suzuki, E. Kuranaga, O. Ohara, M. Miura, Single-cell imaging of caspase-1 dynamics reveals an all-or-none inflammasome signaling response, Cell Rep. 8 (4) (2014) 974–982.

[43] E. Bartok, F. Bauernfeind, M.G. Khaminets, C. Jakobs, B. Monks, K.A. Fitzgerald, E. Latz, V. Hornung, iGLuc: a luciferase-based inflammasome and protease activity reporter, Nat. Methods 10 (2) (2013) 147–154.

[44] D.L. Jasinski, H. Yin, Z. Li, P. Guo, Hydrophobic effect from conjugated chemicals or drugs on in vivo biodistribution of RNA nanoparticles, Hum. Gene Ther. 29 (1) (2018) 77–86.